Ordering of divalent cations in the apatite structure: Crystal structure refinements of natural Mn- and Sr-bearing apatite

JOHN M. HUGHES, MARYELLEN CAMERON, KEVIN D. CROWLEY

Department of Geology, Miami University, Oxford, Ohio 45056, U.S.A.

ABSTRACT

High precision ($R \leq 0.021$) single-crystal structure refinements of four apatite samples were undertaken to elucidate the ordering of Mn and Sr in natural apatite and to determine the structural response to substitution of these divalent ions in the apatite atomic arrangement. The crystals studied were naturally occurring and had compositions ($Mn_{1.21}$, $Mn_{0.42}$, $Sr_{0.63}$, and $Sr_{0.29}$ atoms/ten Ca sites) typical of apatite in many igneous, metamorphic, and sedimentary rocks.

In contrast to the findings of a previous Rietveld study, the symmetry of Mn-bearing apatite does not degenerate from $P6_3/m$ to $P6_3$ or $P3$ with Mn substitution, nor does degenerate symmetry limit Mn substitution to one atom/unit cell. The substituent Mn^{2+}, which is smaller than Ca^{2+}, preferentially occupies the larger apatite Ca1 site although not completely. The Mn atom is underbonded in either Ca site but less so in the larger Ca1 site; the nine O atoms coordinating that site more effectively satisfy the Mn bond valence than the seven ligands of the Ca2 site. M-O bond lengths of the Mn-substituted sites reflect the substitution of the smaller Mn ion.

The Sr^{2+} ion, which is larger than Ca^{2+}, is ordered almost completely into the smaller Ca2 site in the apatite structure. Bond valence sums of the Sr ion in the two sites demonstrate that Sr is severely overbonded in either apatite Ca site but less so in the Ca2 site. The complete ordering of Sr into the Ca2 sites has important implications for diffusion of that element in the apatite structure, the subject of several recent studies. Diffusion of Sr in (001) has been shown to be as rapid or more rapid than diffusion parallel to [001]. As there are no sites available to Sr that are linked in (001) nor any interstitial sites that can contain the Sr^{2+} ion, a diffusion mechanism involving vacancies or defects or both is indicated.

INTRODUCTION

Numerous mineralogical studies have addressed the ordering of anions and cations in the apatite structure. In calcium phosphate apatite, the difference in size and bonding ligands (Ca-O vs. Ca-O, F, Cl, OH) of the two crystallographically distinct Ca sites enables extensive substitutions involving both divalent and trivalent cations to occur. Among divalent cations, the most common substituents in natural apatite are Mn^{2+} and Sr^{2+}.

The presence and behavior of Sr in the apatite structure are important in petrologic studies, especially ones that involve Rb-Sr isotope systematics or trace element modeling of granitoid systems. Recent experimental studies that address the behavior of Sr in apatite include those of Farver and Giletti (1989) and Watson et al. (1985) on diffusion of Sr in apatite, and Watson and Green (1981) on partitioning of Sr between apatite and melt. Crystallographic and spectroscopic studies that examine ordering of Sr between the two Ca sites provide conflicting results.

Mn-bearing apatites have for many years been of special interest to materials scientists in the fluorescent light-ing industry. More recently, Suitch et al. (1985) noted that the presence of minor amounts of Mn in phosphate ores may be a potentially important source of Mn because of the large volumes of phosphate ores processed annually. Crystallographic research results on the ordering of Mn^{2+} are also contradictory.

In this paper, we present the results of four crystal structure refinements of Mn- and Sr-bearing apatite samples. Our study involves natural materials and emphasizes compositional variants typical of many igneous, metamorphic, and sedimentary occurrences. These data are among the first high-precision refinements obtained specifically to address the ordering of Mn and Sr within the apatite atomic arrangement.

PREVIOUS WORK

Numerous experiments, with contradictory results, have addressed the ordering of substituent Sr and Mn cations between the two nonequivalent Ca sites (Ca1, Ca2) in apatite. In a predictive study based on energy analysis of cation ordering in apatite, Urusov and Khudolozhkin (1975) suggested that the "high" preference of Mn^{2+} for

TABLE 1. Crystal data and results of crystal structure refinements for Sr- and Mn-bearing apatite

	$Sr_{0.63}$	$Sr_{0.29}$	$Mn_{1.21}$	$Mn_{0.42}$
Size (mm)	$0.16 \times 0.15 \times 0.14$	$0.16 \times 0.16 \times 0.20$	$0.17 \times 0.10 \times 0.08$	$0.16 \times 0.13 \times 0.08$
Unit-cell dimensions				
Least squares				
a (Å)	9.391(2)	9.377(2)	9.344(2)	9.361(1)
b (Å)	9.390(1)	9.380(2)	9.342(2)	9.358(1)
c (Å)	6.9011(8)	6.8922(7)	6.823(1)	6.860(1)
α (°)	89.97(1)	90.00(1)	90.05(1)	89.98(1)
β (°)	90.03 (1)	90.01(1)	89.98(1)	90.02(1)
γ (°)	120.02(1)	119.97(1)	119.98(1)	120.01(1)
Structure refinement ($P6_3/m$)				
a (Å)	9.3902	9.3786	9.3430	9.3596
c (Å)	6.9011	6.8922	6.8227	6.8603
θ range	0.5–30°	0.5–30°	0.1–30°	0.1–30°
Reflections	$\pm h + k + l$	$\pm h + k + l$	$\pm h \pm k + l$	$\pm h + k + l$
Scan time	≤ 75 s	≤ 80 s	≤ 70 s	≤ 90 s
Scan type	$\theta/2\theta$	$\theta/2\theta$	$\theta/2\theta$	$\theta/2\theta$
Number of data	1740	1737	3225	1731
Unique data	557	557	545	554
R_{merge}	0.016	0.021	0.023	0.017
Reflections $I > 3\sigma_I$	433	448	373	419
Refined parameters	42	42	42	42
R	0.015	0.021	0.017	0.015
R_w	0.023	0.026	0.021	0.020
$\Delta\rho$ residua (e Å^{-3})				
(+)	0.422	0.377	0.325	0.308
(−)	0.413	0.470	0.329	0.310

Note: For Table 1 and subsequent tables, numbers in parentheses denote 1 esd of the least significant digit.

the Ca1 site and the "medium" preference of Sr for the Ca2 site in fluor- and hydroxylapatite results from the differing electronegativity of the ligands of the two sites, i.e., Ca1-O_9 vs. Ca2O_6X (where X = F, OH). In a structure analysis of a synthetic strontium apatite [$Sr_3Ca_2(PO_4)_3F$], Klevcova (1964) demonstrated that the symmetry of the compound degenerates to $P6_3$ from the $P6_3/m$ of end-member fluorapatite and that the Sr atoms are distributed between the degenerate equivalents of both $P6_3/m$ sites. Klevcova and Borisov (1964) reported the structure of belovite [$NaCeSr_3(PO_4)_3(OH)$] and concluded that the Sr is ordered solely into the Ca2 sites, with degenerate symmetry of $P\bar{3}$ that results from ordering of the Na and Ce atoms. Khudolozhkin et al. (1972) synthesized a series of Sr-substituted hydroxylapatite samples and determined the ordering of Sr between the two cation sites based on the intensity ratios derived from eight reflections measured using a powder diffractometer. They concluded that Sr preferentially occupies the Ca2 sites in apatite with ~10% Sr substitution but that the degree of ordering decreases as the Sr content increases. Heijligers et al. (1979) and Andres-Verges et al. (1980) suggested, on the basis of powder X-ray and infrared spectra, respectively, that the Sr occupies both Ca sites in Sr-substituted synthetic hydroxylapatite, but the ratio Sr_{Ca1}/Sr_{Ca2} varies as a function of composition.

Numerous studies, also with contradictory results, have been undertaken to determine the ordering of Mn^{2+} between the two Ca sites in the apatite atomic arrangement. In a summary of studies that were undertaken using electron paramagnetic resonance, thermoluminesence, and infrared spectroscopic techniques, Suitch et al. (1985) noted that Mn^{2+} substitutes for Ca^{2+} at the Ca1 site ex-

clusively or preferentially. The Suitch et al. study, which employed neutron diffraction and the Rietveld method on synthesized powders with ~$\frac{3}{8}$ Mn^{2+} atoms/unit cell, concluded that the Mn-substituted $P6_3/m$ apatite structure degenerates to at least $P6_3$ and perhaps $P3$ and that the Mn atoms occupy a subset of the $P6_3/m$ Ca1 sites. Furthermore, their results suggested that rotations of the PO_4 groups in response to local substituent Mn atoms limit Mn substitution to a maximum of one Mn^{2+}/unit cell (i.e., per ten Ca sites), a maximum in accord with that observed in a previous infrared spectroscopic study. It should be noted, however, that in the Suitch et al. study occupancy was not modeled using thermal neutron scattering factors for Mn and Ca but by refining Ca multiplicity factors and thus inferring site occupancy. In addition, in none of the three model space groups ($P6_3/m$, $P6_3$, $P3$) were they able to refine all anisotropic thermal parameters to positive, definite values.

EXPERIMENTAL

The analyzed specimens of Mn-bearing apatite are from Branchville, Connecticut (American Museum of Natural History no. AMNH C69824), and from the Harding pegmatite, Taos County, New Mexico (Northrup et al., 1989). Microprobe analysis (Dwight Deuring, Southern Methodist University, analyst) of the former gave 6.81 wt% MnO and yielded unit-cell contents of $(Ca_{8.81}Mn_{1.00}Fe_{0.10}Na_{0.07}Ce_{0.02})_{10.00}P_{6.00}O_{24}(F_{1.48}OH_{0.52})$, whereas the X-ray refinement gave 1.21 Mn atoms/unit cell for the same crystal. The disparity between the microprobe value (1.00 Mn atoms) and the refinement value (1.21 Mn atoms) is probably due in large part to the 0.10 Fe and 0.02 Ce atoms/unit cell. Microprobe analysis of

TABLE 2. Positional parameters and equivalent isotropic temperature factors (Å²) for Sr- and Mn-bearing apatite samples

	x	y	z	B
Ca1				
$Sr_{0.63}$	2/3	1/3	0.00086(9)	0.850(7)
$Sr_{0.29}$	2/3	1/3	0.00092(9)	0.732(8)
$Mn_{1.21}$	2/3	1/3	0.0021(1)	0.947(9)
$Mn_{0.42}$	2/3	1/3	0.00155(9)	0.828(6)
Ca2				
$Sr_{0.63}$	−0.00854(5)	0.24046(5)	1/4	0.792(8)
$Sr_{0.29}$	−0.00788(5)	0.24114(5)	1/4	0.670(8)
$Mn_{1.21}$	−0.00708(7)	0.24151(7)	1/4	0.88(1)
$Mn_{0.42}$	−0.00704(5)	0.24157(5)	1/4	0.751(7)
P				
$Sr_{0.63}$	0.36912(7)	0.39843(7)	1/4	0.60(1)
$Sr_{0.29}$	0.36899(7)	0.39827(7)	1/4	0.51(1)
$Mn_{1.21}$	0.36997(9)	0.39878(9)	1/4	0.71(1)
$Mn_{0.42}$	0.36937(6)	0.39843(6)	1/4	0.573(9)
O1				
$Sr_{0.63}$	0.4846(2)	0.3269(2)	1/4	0.95(3)
$Sr_{0.29}$	0.4852(2)	0.3272(2)	1/4	0.90(3)
$Mn_{1.21}$	0.4883(2)	0.3298(2)	1/4	1.19(4)
$Mn_{0.42}$	0.4859(2)	0.3273(2)	1/4	0.97(3)
O2				
$Sr_{0.63}$	0.4665(2)	0.5877(2)	1/4	1.13(4)
$Sr_{0.29}$	0.4670(2)	0.5879(2)	1/4	0.98(3)
$Mn_{1.21}$	0.4656(3)	0.5882(3)	1/4	2.01(6)
$Mn_{0.42}$	0.4666(2)	0.5882(2)	1/4	1.29(3)
O3				
$Sr_{0.63}$	0.2574(1)	0.3416(2)	0.0711(2)	1.26(2)
$Sr_{0.29}$	0.25737(1)	0.3418(2)	0.0706(2)	1.16(2)
$Mn_{1.21}$	0.2581(2)	0.3406(2)	0.0702(3)	1.87(3)
$Mn_{0.42}$	0.2575(1)	0.3414(1)	0.0707(2)	1.39(2)
F				
$Sr_{0.63}$	0	0	1/4	2.00(5)
$Sr_{0.29}$	0	0	1/4	1.93(5)
$Mn_{1.21}$	0	0	1/4	2.31(7)
$Mn_{0.42}$	0	0	1/4	1.87(4)

TABLE 4. Selected bond lengths for Mn- and Sr-bearing apatite (Å)

	$Sr_{0.63}$	$Sr_{0.29}$	$Mn_{1.21}$	$Mn_{0.42}$
Ca1–O1 (×3)	2.404(1)	2.398(1)	2.363(2)	2.382(1)
O2 (×3)	2.457(2)	2.457(2)	2.435(2)	2.447(2)
O3 (×3)	2.810(1)	2.804(1)	2.807(2)	2.803(1)
Mean	2.557	2.555	2.535	2.544
Ca2–O1	2.687(2)	2.691(2)	2.712(2)	2.694(1)
O2	2.388(2)	2.376(2)	2.375(2)	2.371(2)
O3 (×2)	2.357(2)	2.352(2)	2.324(2)	2.343(1)
O3′ (×2)	2.507(1)	2.502(1)	2.491(2)	2.491(1)
F	2.2991(5)	2.2993(5)	2.2903(7)	2.2947(5)
Mean$_{oxy}$	2.467	2.464	2.453	2.456
P–O1	1.534(2)	1.536(2)	1.534(3)	1.537(2)
O2	1.540(2)	1.541(2)	1.533(2)	1.539(2)
O3 (×2)	1.533(1)	1.533(1)	1.525(2)	1.528(1)
Mean	1.535	1.536	1.529	1.533

$Mn_{0.01}Ce_{0.02})_{10.10}(P_{5.86}Si_{0.04})_{5.90}O_{24}(F_{1.78}OH_{0.22})$, in contrast to 0.29 Sr atoms/unit cell by X-ray refinement. In the following tables these samples are labeled $Sr_{0.63}$ and $Sr_{0.29}$ respectively, on the basis of their Sr content per unit cell as obtained from the X-ray refinement.

Each crystal was examined using precession methods to confirm hexagonal symmetry (Laue group $6/m$) and the absence of superstructure reflections. Unit-cell parameters were refined (no symmetry constraints) using diffraction angles from 25 automatically centered diffractions, measured on an Enraf-Nonius CAD4 single-crystal diffractometer. Intensity data were measured on the same instrument, and either three or six symmetry-equivalent reflections were measured for each diffraction (Table 1). Absorption was corrected using an empirical ψ-scan technique (North et al., 1968) employing intensity data obtained from 360° ψ scans collected at 10° intervals. Details of data measurements and structure refinements are listed in Table 1.

Crystal structure calculations were undertaken in space group $P6_3/m$ using the SDP set of programs (Frenz, 1985). Neutral-atom scattering factors were employed, including terms for anomalous dispersion. Reflections with $I < 3\sigma_I$ were considered unobserved, and observed reflections were weighted proportional to σ_I^{-2}, with a term to downweigh intense reflections. Full-matrix least-squares refinement was undertaken by refining positional parameters, a scale factor, anisotropic temperature factors, an isotropic extinction factor, and site occupancy for the Ca1 and Ca2 sites using the fluorapatite data of Hughes et al. (1989) as starting parameters. For all crystals, column anions were modeled using only F because of the small amount of OH present.

Table 2 contains positional parameters and isotropic temperature factors for the four structures, and Table 3[1] presents anisotropic temperature factors. Table 4 contains selected bond distances, and Table 5 gives occupancies of

the Harding pegmatite sample used in the structure study gave 2.81 wt% MnO and unit-cell contents of $(Ca_{9.59}Mn_{0.41}Sr_{0.01}Na_{0.01})_{10.02}P_{5.98}O_{24}(F_{1.86}OH_{0.14})$, in contrast to 0.42 Mn atoms/unit cell by X-ray refinement. In the following tables, these samples are labeled $Mn_{1.21}$ and $Mn_{0.42}$, respectively, on the basis of their Mn content per unit cell as obtained from the X-ray refinement.

Although Sr enters the apatite structure in amounts significant enough to form unique minerals (e.g., belovite), we chose to analyze natural Sr-substituted fluorapatites with Sr concentrations typical of geologic samples. Specimens of Sr-bearing apatite from the Kola Peninsula were obtained from the Smithsonian Institution (SM113855) and from the American Museum of Natural History (AMNH 35876). The individual crystals used in the X-ray refinement were analyzed by electron microprobe (Dwight Deuring, Southern Methodist University, analyst). The analysis of the Smithsonian crystal used for structure refinement gave 3.83 wt% SrO and yielded unit-cell contents of $(Ca_{9.53}Sr_{0.40}Na_{0.09}Ce_{0.06})_{10.08}(P_{5.87}Si_{0.06})_{5.93}O_{24}$-$(F_{2.18})$. The X-ray refinement yielded 0.63 Sr atoms/unit cell; we attribute the disparity between the X-ray and microprobe results to analytical error and to the presence of 0.06 Ce atoms/unit cell. Microprobe analysis of the AMNH specimen used in the X-ray study gave 2.70 wt% SrO and yielded unit-cell contents of $(Ca_{9.75}Sr_{0.27}Na_{0.05}$-

---

[1] Copies of Tables 3 and 6 may be ordered as Document AM-91-482 from the Business Office, Mineralogical Society of America, 1130 Seventeenth Street NW, Suite 330, Washington, DC 20036, U.S.A. Please remit $5.00 in advance for the microfiche.

TABLE 5. Site occupancies for Mn- and Sr-bearing apatite

	Total Mn*	Mn/site	Valence sum for Mn**
	Mn$_{1.21}$		
Ca1	0.82(3)	0.21	1.44
Ca2	0.39(3)	0.07	1.31
Total	1.21		
	Mn$_{0.42}$		
Ca1	0.33(2)	0.08	1.41
Ca2	0.09(2)	0.02	1.29
Total	0.42		
	Total Sr*	Sr/site	Valence sum for Sr**
	Sr$_{0.63}$		
Ca1	0.066(7)	0.017	2.94
Ca2	0.563(9)	0.094	2.70
Total	0.629		
	Sr$_{0.29}$		
Ca1	0.007(7)	0.002	2.97
Ca2	0.288(9)	0.048	2.75
Total	0.295		

* Values obtained from X-ray refinement.
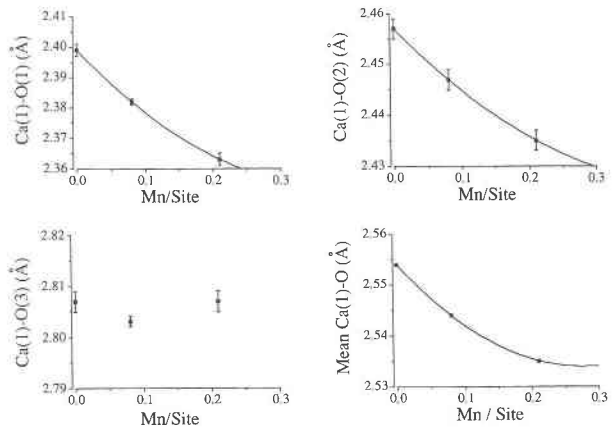** Valence sums in valence units.

Fig. 1. Variation of Ca1-O bond lengths with substituent Mn. Datum with Mn = 0.0 is fluorapatite of Hughes et al. (1989). Best-fit second order curve through data is denoted.

the Ca sites in the apatite structures. Table 6 gives observed and calculated structure factors.

DISCUSSION OF THE STRUCTURES

Mn-bearing apatite

The structure refinements of Mn-bearing apatite do not support the suggestion that apatite symmetry degenerates to $P6_3$ or $P3$ with inclusion of small amounts of Mn^{2+} (Suitch et al., 1985). Both apatite structure refinements were well behaved in space group $P6_3/m$, as illustrated in reasonable thermal parameters, smooth convergence of all parameters, small R_{merge} values in space group $P6_3/m$, and final refinement R values ≤0.017 (Table 1). Thus we report all data for space group $P6_3/m$ for lack of evidence to the contrary.

Suitch et al. (1985) also suggested that the upper compositional limit for Mn-bearing apatite is one atom/unit cell, corresponding to 6.9 wt% for Mn-bearing fluorapatite. However, in microprobe analyses of Mn-bearing apatite we have found concentrations as high as 7.3 wt%, and an unpublished study by Miller and others (Mary K. Roden, personal communication) yielded apatite with up to 7.87(4) wt% MnO, giving 1.17 Mn atoms/unit cell. In addition, other published analyses present MnO concentrations of 7.59 wt%, yielding 1.09 Mn atoms/unit cell (Deer et al., 1962). These results suggest that the putative one atom/unit cell limit for Mn occupancy may not be real.

In the Mn-bearing apatite samples examined in this study, Mn displays a distinct preference for the apatite Ca1 site, although it is not excluded from the Ca2 site. Table 5 presents the Mn occupancy for the Ca1 and Ca2 sites in both apatite crystals studied. As shown there, the Ca1 site contains 0.82 of the 1.21 total Mn atoms for the Branchville specimen and 0.33 of the 0.42 Mn atoms for the Harding pegmatite sample.

Mn^{2+} has a $3d^5$ valence electron configuration and can occur in either a high-spin or a low-spin state. However, as noted by Peacor (1972), for the coordinating ligands normally found in natural minerals (including O^{2-}, OH^-, Cl^-, and F^-, the ligands for the Ca1 or Ca2 sites in apatite), the crystal field is relatively weak and thus only the high-spin case occurs. Thus, the $t_{2g}^3 e_g^2$ electron configuration yields no crystal field stabilization energy, and only radius and site geometry should control Mn substitution in the apatite structure.

Despite substitution by numerous elements in the apatite Ca sites, Mn^{2+} is the only divalent, period-4 element to substitute in the sites to any extent. For sevenfold coordination, the coordination of the Ca2 site in apatite, Shannon (1976) gives a radius value of 0.90 Å for high-spin $^{[7]}Mn^{2+}$, in contrast to a value of 1.06 Å for $^{[7]}Ca^{2+}$. For ninefold coordination, approximating the crystal field for the Ca1 site in apatite, values are not available for Mn. The size contrast between Ca and Mn results in a significant effect on the bonding at the apatite Ca sites. Table 5 gives bond valence sums for Mn^{2+} in the two sites (calculated using the constants of Brown, 1981). These data show that Mn is underbonded in either Ca site although less so in the Ca1 site. (It should be noted that the bond valence sums were calculated using the average M site, as different sites for Ca and Mn were not distinguished.) Although the Ca1 site is the larger of the Ca sites in the apatite structure in terms of average bond length, its coordination to nine O atoms (vs. seven ligands for the Ca2 site) more closely satisfies the formal charge of the Mn ion. It is interesting to note that apatite effectively acts as a geochemical sieve that traps Mn^{2+} and excludes Fe^{2+}, elements that are virtually inseparable in most geochemical systems. Bond valence sums for Fe^{2+} in the apatite Ca sites yield 1.26 and 1.19 valence units for the Ca1 and Ca2 sites, respectively; the large discrepancy from the formal valence prohibits extensive substitution of Fe^{2+} in the apatite structure.

The response of the calcium apatite structure to Mn^{2+} substitution is evident in both Ca coordination polyhedra. Figure 1 displays bond lengths for the Mn-substituted Ca1 site, which is the site with the higher Mn concentration; the figure also shows the fluorapatite data of Hughes et al. (1989) for comparison. With increasing Mn content, the shorter Ca1-O1 and Ca1-O2 bond lengths decrease nearly linearly. The length of the significantly longer and weaker Ca1-O3 bond remains approximately constant with these levels of Mn substitution. The mean Ca1-O distances for both Mn-substituted structures are smaller than that of fluorapatite (2.535 Å and 2.544 Å vs. 2.554 Å). With increasing Mn content, variations in individual bonds in the Ca2 polyhedron are irregular. Both long Ca2-O1 and short Ca2-O3 bonds change significantly but in opposite directions. Mean Ca2 distances are essentially identical for the two manganese apatite samples and slightly shorter than that of the fluorapatite of Hughes et al. (1989) (e.g., 2.453 Å and 2.456 Å vs. 2.463 Å).

Sr-bearing apatite

The Sr^{2+} ion is significantly larger than the Ca^{2+} ion. Shannon (1976) gave radii values of 1.31 Å for $^{[9]}Sr^{2+}$ and 1.21 Å for $^{[7]}Sr^{2+}$; these values compare with 1.18 Å and 1.06 Å for $^{[9]}Ca^{2+}$ and $^{[7]}Ca^{2+}$ for Ca in coordination of the apatite Ca1 and Ca2 sites, respectively.

The several studies cited previously are contradictory with regard to ordering of substituent Sr in the apatite structure. The results of this study demonstrate that in these natural samples of geologically typical Sr abundance, Sr^{2+} is ordered almost completely into the apatite Ca2 sites. Table 5 presents the Sr occupancy of the two apatite cation sites. As shown therein, only 0.07 Sr atoms occur in the Ca1 sites in the sample with 0.63 Sr atoms, and 0.007 Sr atoms occur in the Ca1 site in the sample with 0.29 Sr atoms/unit cell. The reason for the observed ordering is evident from calculations of bond valence sums for Sr in the two apatite sites. Table 5 includes data that indicate that the large Sr ion is grossly overbonded in both Ca sites but less so in the Ca2 site. The results of the X-ray refinements demonstrate that the extreme overbonding for Sr in the Ca1 site (one valence unit greater than the formal valence) cannot be overcome by structural adjustments involving O atoms, and thus Sr is ordered almost exclusively into the Ca2 site.

The ordering of Sr into the apatite Ca2 site provides constraints on the mechanisms of diffusion of Sr in apatite. Watson et al. (1985) found that Sr diffusivity rates were greater perpendicular to the c axis than parallel to the c axis. Although the differences in diffusion rates were small, they were larger than the precision of the measurements. Farver and Giletti (1989) observed minor anisotropy for Sr diffusion in apatite, although they noted that their results are too scattered to contradict the Watson et al. conclusion of diffusion anisotropy at temperatures exceeding 1050 °C.

In the apatite structure, the Ca2 sites are hexagonally disposed about the central anion column. Adjacent Ca2
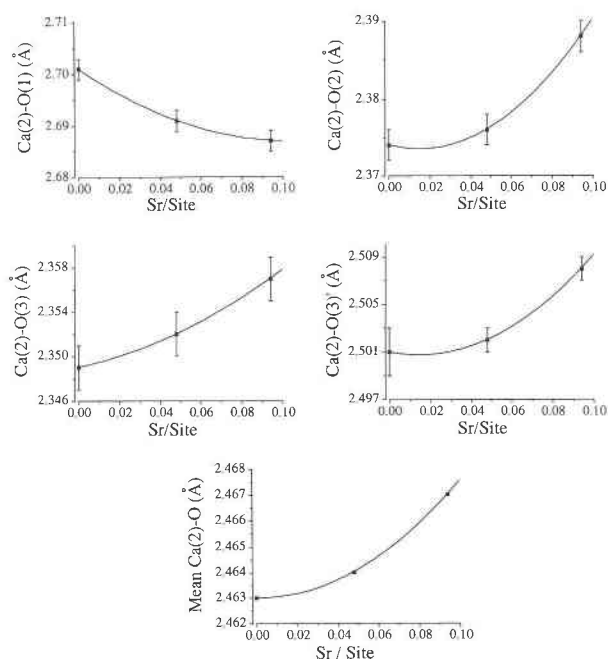

Fig. 2. Variation of Ca2-O bond lengths with substitution of Sr. Datum with Sr = 0.0 is fluorapatite of Hughes et al. (1989). Best-fit second order curve through data is denoted.

sites related by the 6_3 axis are linked through a shared O3 atom. In fluorapatite, the adjacent Ca2 sites are separated by a distance of 4.14 Å and form a helix of linked polyhedra whose axis is parallel to c. This helix of linked sites provides a structural framework that allows volume diffusion of Sr by an exchange mechanism between adjacent Ca2 sites or by migration of vacancies along the chain. In contrast, diffusion in (001) is hampered by the surrounding cation polyhedra. The central channel of Ca2 sites, which contains the substituent Sr ions, is surrounded by polyhedra in (001) for which Sr is excluded, i.e., the P and Ca1 sites. Transport by means of jumps involving interstitial sites is also unlikely. To test for the existence of interstitial sites that could accommodate the Sr^{2+} ion, we calculated the ligation of all interstitial sites in the fluorapatite structure on a grid of 0.1 × 0.1 × 0.1 Å. In the room-temperature structure, no interstitial sites exist that are capable of containing the Sr ion, as all such sites are less than 2.2 Å from an O atom. Thus, if diffusion rates are indeed equal or faster in (001) than parallel to [001], diffusion must be aided by vacancies or structural defects, as movement through interstitial sites is not a viable diffusion mechanism in the apatite atomic arrangement.

The response of the calcium apatite structure to Sr^{2+} substitution on the order of 0.29 and 0.63 atoms/ten Ca sites is significant only in the Ca2 site. Figure 2 displays bond distances for Ca2, which is the site containing most of the Sr. With increasing Sr, the relatively short Ca2-O2, -O3, -O3' bonds exhibit small increases (0.005–0.012 Å) in length, whereas the longer and weaker Ca2-O1 bond

exhibits a small decrease (Fig. 2). The mean Ca2-O distances for both Sr-substituted apatite samples are not significantly different and are comparable to that of the fluorapatite studied by Hughes et al. (1989) (2.467 Å and 2.464 Å vs. 2.463 Å). Bond distances for the Ca1 polyhedron of both strontium apatite samples included in this study and the fluorapatite of Hughes et al. (1989) are very similar (2.557 Å and 2.555 Å vs. 2.554 Å).

ACKNOWLEDGMENTS

REFERENCES CITED

Andres-Verges, M., Higes-Rolandi, F.J., and Gonzalez-Diaz, P.F. (1980) Is there a continuous cation migration in calcium-strontium hydroxyapatites? Journal of Solid State Chemistry, 33, 125–126.

Brown, I.D. (1981) The bond-valence method: An empirical approach to chemical structure and bonding. In M. O'Keeffee and A. Navrotsky, Eds., Structure and bonding in crystals II, p. 1–30. Academic Press, New York.

Deer, W.A., Zussman, J., and Howie, R.A. (1962) Rock-forming minerals, vol. 5: Non-silicates. Longman, London.

Farver, J.R., and Giletti, B.J. (1989) Oxygen and strontium diffusion kinetics in apatite and potential applications to thermal history determination. Geochimica et Cosmochimica Acta, 53, 1621–1631.

Frenz, B.A. (1985) Enraf-Nonius structure determination package. SDP users guide, version 4. Enraf-Nonius, Delft, The Netherlands.

Heijligers, H.J.M., Verbeeck, R.M.H., and Driessens, F.C.M. (1979) Cation distribution in calcium-strontium-hydroxyapatites. Journal of Inorganic and Nuclear Chemistry, 41, 763–764.

Hughes, J.M., Cameron, M., and Crowley, K.D. (1989) Structural variations in natural F, OH, and Cl apatites. American Mineralogist, 74, 870–876.

Khudolozhkin, V.O., Urusov, V.S., and Tobelko, K.I. (1972) Ordering of Ca and Sr in cation positions in the hydroxylapatite-belovite isomorphous series. Geokhimiya, 10, 1236–1244.

Klevcova, R.F. (1964) The crystal structure of strontium apatite. In W.B. Pearson, Ed., Structure reports, vol. 29, p. 370. Bohn, Scheltema, and Hokema, Utrecht, The Netherlands.

Klevcova, R.F., and Borisov, S.V. (1964) The crystal structure of belovite. In W.B. Pearson, Ed., Structure reports, vol. 29, p. 374. Bohn, Scheltema, and Hokema, Utrecht, The Netherlands.

North, A.C.T., Phillips, D.C., and Matthews, F.S. (1968) A semi-empirical method of absorption correction. Acta Crystallographica, A24, 351–359.

Northrup, C.J., Lumpkin, G.R., and Ewing, R.C. (1989) Variation in the composition of beryl and apatite from the Harding Pegmatite, Taos County, New Mexico. Geological Society of America Abstracts with Programs, 21, A198–A199.

Peacor, D.R. (1972) Manganese: Crystal chemistry. In K.H. Wedepohl, Ed., Handbook of geochemistry, vol. II-3, p. 25-A-1–25-A-12. Springer-Verlag, New York.

Shannon, R.D. (1976) Revised effective ionic radii and systematic studies of interatomic distances in halides and chalcogenides. Acta Crystallographica, A32, 751–767.

Suitch, P.R., LaCout, J.L., Hewat, A., and Young, R.A. (1985) The structural location and role of Mn^{2+} partially substituted for Ca^{2+} in fluorapatite. Acta Crystallographica, B41, 173–179.

Urusov, V.S., and Khudolozhkin, V.O. (1975) An energy analysis of cation ordering in apatite. Geochemistry International, 11, 1048–1053.

Watson, E.B., and Green, T.H. (1981) Apatite/liquid partition coefficients for the rare earth elements and strontium. Earth and Planetary Science Letters, 56, 405–421.

Watson, E.B., Harrison, T.M., and Ryerson, F.J. (1985) Diffusion of Sm, Sr, and Pb in fluorapatite. Geochimica et Cosmochimica Acta, 49, 1813–1823.